AMERICAN JOURNAL OF APPLIED MEDICAL SCIENCE
ISSN: 2996-5101 (online) | ResearchBib (IF) = 10.81 IMPACT FACTOR
Volume-3| Issue-8| 2025 Published: |30-09-2025|

COMPARATIVE STUDY OF THE EFFECTS OF RUTAN AND CARSIL ON STRUCTURAL CHANGES IN THE LIVER IN PREPUBERTAL RATS WITH ACUTE TOXIC HEPATITIS

https://doi.org/10.5281/zenodo.17180670

Khakimov Ziyaviddin Zaynutdinovich[1]
Rakhmanov Alisher Khudaiberdievich[2]
Khalmuratova Fatima Adilbaevna[3]
Abduvaliev Abdurakhmon Rustamovich[4]

[1] Doctor of Medical Sciences, Professor, Department of Pharmacology, Tashkent State Medical University, Uzbekistan [2] Doctor of Medical Sciences, Professor, Senior Researcher, Center for Biomedical Technologies, Tashkent State Medical University, Uzbekistan [3] Assistant, Department of Pharmacology and Pharmaceutical Technology, Karakalpak Medical Institute, Uzbekistan [4] Junior Researcher, Center for Biomedical Technologies, Tashkent State Medical University, Uzbekistan

Introduction. The liver plays a multifaceted role in the body, as it is involved not only in digestive processes but also in all types of metabolic pathways. According to WHO data, there is a clear global trend toward an increasing prevalence of hepatobiliary diseases, which contribute to high mortality rates [1]. Despite the availability of a wide range of therapeutic agents, the search for new effective treatments aimed at correcting morphofunctional liver disorders of various etiologies continues, based on the results of in-depth experimental studies.

Rutan has been introduced into clinical practice as an antiviral agent with the ability to stimulate endogenous interferon production [2,3]. Experimental studies have demonstrated that this drug possesses anti-inflammatory and hepatoprotective properties [4–7]. At the same time, it should be noted that the clinical efficacy of many well-known and long-used hepatoprotective agents has not been conclusively proven [8].

Our previous studies demonstrated the effectiveness of Rutan in treating acute toxic hepatitis in prepubertal animals [9–12]; however, its effects on liver structure have not yet been investigated.

The aim of the present study was to examine the effect of Rutan on liver structure in acute toxic hepatitis in prepubertal animals.

Materials and Methodsıo Acute toxic hepatopathy was induced in male rats by intragastric administration of a 50% oil solution of carbon tetrachloride (CCl_4) at a dose of 0.2 mL per 100 g body weight once daily for four consecutive days [13]. Twenty-four hours after the last CCl_4 administration, the animals were randomly

divided into four experimental groups. The first group consisted of healthy animals that received no intervention and served as a normal control (Group A). The second group included rats exposed to CCl_4 without therapeutic treatment, serving as a pathological control (Group B). The third group received the reference hepatoprotective drug Carsil at a dose of 40 mg/kg once daily for six days (Group C). The fourth group was treated with the experimental formulation Rutan at a dose of 25 mg/kg, also administered once daily for six days (Group D). Twenty-four hours after the last administration, all animals were euthanized by decapitation under light ether anesthesia.

Liver samples were fixed in 12% neutral buffered formalin for at least 24 hours, trimmed to 3–4 mm thickness, and processed according to standard paraffin embedding protocols. Samples were dehydrated through a graded ethanol series (70%, 80%, 95%, 100% ×2), cleared in xylene (two changes), and infiltrated with paraffin at 60 °C (two changes). Tissue blocks were oriented according to lobular architecture and allowed to solidify on a cold plate. Sections of 6–8 µm thickness were cut on a microtome, floated on a water bath at 40–45 °C, mounted on positively charged slides, and dried overnight at 37–42 °C. Hematoxylin and eosin (H&E) staining was performed using standard laboratory protocols: deparaffinization in xylene (2 × 5 min), rehydration through a descending ethanol series (100% ×2, 95%, 80%, 70%), washing in running water, staining with Harris hematoxylin (3 min), brief differentiation in acid alcohol (10 s), washing, and counterstaining with eosin Y (40 s). Stained sections were dehydrated through ascending ethanol concentrations, cleared in xylene (two changes), and mounted in a resinous medium under a coverslip. Stained specimens were examined using a Leica DM IL LED microscope equipped with a 10× ocular lens and 10×, 20×, and 40× objectives, corresponding to the above total magnifications. Histological analysis was performed at three levels: lower magnification (total magnification – 100×), intermediate magnification (total magnification – 200×), and higher magnification (total magnification – 400×). The total area of red staining in captured images was quantified using Fiji software. For each experimental group, non-overlapping fields were randomly selected and saved in uncompressed TIFF format to preserve image quality.

Mononuclear cell infiltration was quantitatively assessed on images acquired at intermediate magnification. For each experimental animal, 5 randomly selected fields were analyzed. Individual mononuclear cells were counted manually using the Multi-Point tool in Fiji; points were placed on each nucleus to obtain a reproducible count and saved in the ROI Manager for documentation.Identification and Counting of Lipid-Loaded. Hepatocytes Hepatocytes were identified on H&E-

AMERICAN JOURNAL OF APPLIED MEDICAL SCIENCE
ISSN: 2996-5101 (online) | ResearchBib (IF) = 10.81 IMPACT FACTOR
Volume-3| Issue-8| 2025 Published: |30-09-2025|

stained sections based on characteristic cytoplasmic vacuolization and the presence of pyknotic or absent nuclei. Cells meeting these morphological criteria were counted manually on images acquired at higher magnification. For each experimental animal, three randomly selected fields were analyzed. Counting was performed using the Multi-Point tool in Fiji and recorded in the ROI Manager for verification. Reported values represent the average number of cells per field (or, when indicated, normalized to the field area).

Steatotic Area Measurement. The steatotic (lipid) area in each field was measured on images acquired at low magnification. For each experimental animal, five randomly selected fields were analyzed. For each image, the scale was set as described above, and a rectangular region of interest (ROI) was used to define the analyzed field. Steatotic areas were manually segmented by outlining the pale vacuolated regions corresponding to lipid accumulations; each ROI was saved in the ROI Manager. The area of each steatotic ROI was measured in μm^2 and summed to obtain the total steatotic area per image. Final measurements were calculated per field and per animal as required, and steatosis load was expressed either as the total steatotic area or normalized values.

Results and Discussion. At low magnification (10× objective), liver sections from the intact control group exhibited well-preserved lobular architecture characteristic of normal hepatic tissue. Classical hexagonal lobules were clearly delineated, with centrally located central veins and radiating plates of uniform hepatocytes. Hepatocyte cords were arranged regularly, forming single- or double-row trabeculae oriented toward the portal tracts. Sinusoids were evenly distributed, maintaining normal lumen and orientation between hepatocyte plates, with no signs of congestion or collapse. Portal triads—comprising branches of the hepatic artery, portal vein, and bile duct—were intact and properly localized at the periphery of the lobules. Hepatocytes displayed uniformly eosinophilic cytoplasm with centrally positioned, round nuclei and well-defined nucleoli. No signs of cellular degeneration, vacuolization, steatosis, or necrosis were observed. Inflammatory infiltrates were absent, and the connective tissue stroma showed no evidence of fibrosis or ductular reaction. Overall, the liver parenchyma retained normal structural integrity and cellular morphology at this magnification (Figure 3.1, panel A).

AMERICAN JOURNAL OF APPLIED MEDICAL SCIENCE
ISSN: 2996-5101 (online) | ResearchBib (IF) = 10.81 IMPACT FACTOR
Volume-3| Issue-8| 2025 Published: |30-09-2025|

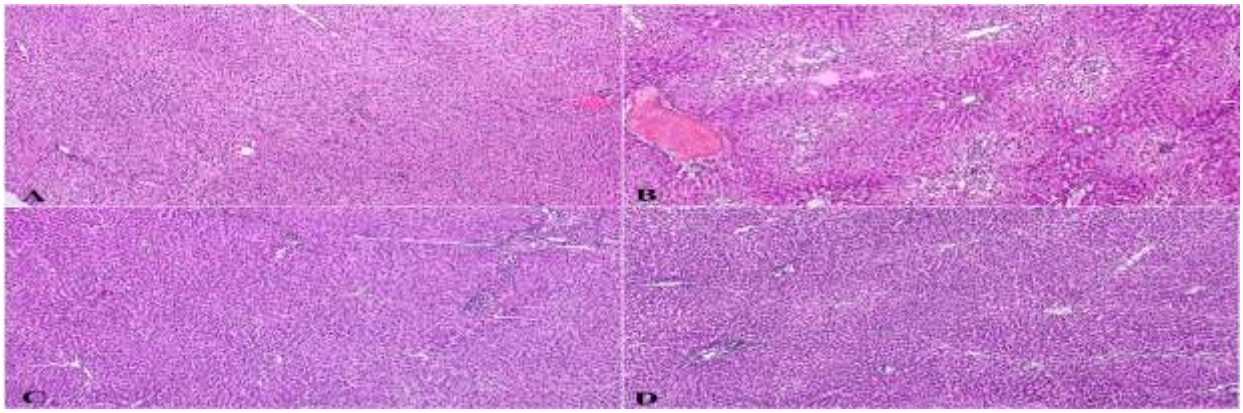

Figure 3.1. Representative liver histology at low magnification across all experimental groups.

In contrast, liver sections from the group exposed to CCl_4 without treatment exhibited pronounced alterations in lobular organization and regional parenchymal integrity at low magnification (Figure 3.1, panel B). The classical hexagonal lobular structure remained partially recognizable; however, in several areas it was disrupted due to parenchymal disorganization and focal collapse. Central veins were identifiable, although in some lobules the surrounding architecture appeared blurred because of structural distortions and irregular sinusoidal arrangement. The most prominent changes were observed in the mid-zonal region, including focal thinning of the hepatocyte layer and loss of uniform hepatocyte cord organization. These areas displayed slight tissue pallor and a vacuolated appearance at low magnification, indicative of lipid degeneration. Scattered foci of hepatocyte dropout were noted, although confluent necrosis was absent. Periportal zones largely retained normal structural features, with intact vascular elements and orderly hepatocyte arrangement. Moderate accumulation of mononuclear inflammatory cells was observed, predominantly in regions adjacent to vacuolar degeneration. These infiltrates were concentrated around sinusoids and in the mid-zonal region, often near the most altered hepatocytes, suggesting a localized immune response in areas of lipid dysregulation. Central veins and portal vascular structures remained largely intact, although sinusoidal dilation was occasionally observed in affected areas (Figure 3.1, panel B).

At low magnification, liver sections from rats treated with Carsil following CCl_4-induced acute toxic hepatitis showed marked improvement in histoarchitecture compared to the untreated group. Although the classical hexagonal lobular organization remained partially disrupted, clear signs of reparative processes and structural reorganization of the hepatic parenchyma were evident. Central veins were well-defined, and the surrounding hepatocyte plates appeared more orderly compared to the disorganized pattern observed in the untreated CCl_4-exposed group. In the mid-zonal region, parenchymal integrity was

AMERICAN JOURNAL OF APPLIED MEDICAL SCIENCE
ISSN: 2996-5101 (online) | ResearchBib (IF) = 10.81 IMPACT FACTOR
Volume-3| Issue-8| 2025 Published: |30-09-2025|

restored, with more uniform hepatocyte arrangement and reduced sinusoidal deformation relative to the focal disintegration and architectural disruption observed in untreated animals. While some hepatocytes still exhibited residual microvesicular changes consistent with mild lipid degeneration, the extent and severity of vacuolar degeneration were considerably lower than in the untreated group. Mononuclear inflammatory infiltrates persisted but were less pronounced and more diffusely distributed than in the untreated group, where dense focal accumulations of immune cells were observed. Inflammatory cells in this group were primarily located within sinusoidal regions, reflecting a regressing inflammatory response compared to the persistent perisinusoidal inflammation seen in untreated animals. Portal and central vascular structures remained intact, and sinusoidal dilation was minimal, indicating improved microcirculatory integrity relative to the more frequent and pronounced alterations observed in untreated animals. Periportal zones exhibited more orderly hepatocyte arrangement, suggestive of early regenerative processes absent or less pronounced in the untreated group (Figure 3.1, panel C).

At low magnification, liver sections from the Rutana-treated group demonstrated overall restored lobular architecture, with discernible hexagonal lobule organization, clearly identifiable central veins, and radially oriented hepatocyte plates. This pattern was generally comparable to that observed in the Carsil-treated group, which also exhibited partial reorganization of hepatic structure. In both groups, disorganization characteristic of untreated animals was markedly reduced, although minor irregularities in lobular contours and hepatocyte plate alignment persisted to varying degrees. In the mid-zonal region, the area most susceptible to CCl_4-induced damage, Rutana-treated sections showed no obvious signs of focal collapse, disintegration, or sinusoidal deformation. Compared to the Carsil group, where residual vacuolar changes and mild architectural disturbances were still present in the mid-zonal region, liver sections from the Rutana group appeared structurally more stable: hepatocyte plates were more compactly arranged, and sinusoidal distribution remained regular. This suggests a lower degree of lipid-associated cellular alterations under Rutana treatment at this stage of analysis. Mononuclear inflammatory infiltrates were minimal and sparsely distributed, similar to the Carsil group; however, in the Rutana group, even fewer inflammatory foci or accumulations were observed within sinusoidal regions. Dense clusters were absent, and Kupffer cells did not exhibit pronounced activity, indicating a less active or already resolved immune response compared to the other groups (Figure 3.1, panel D).

AMERICAN JOURNAL OF APPLIED MEDICAL SCIENCE
ISSN: 2996-5101 (online) | ResearchBib (IF) = 10.81 IMPACT FACTOR
Volume-3| Issue-8| 2025 Published: |30-09-2025|

At intermediate magnification (20× objective), liver sections from the intact control group exhibited a uniform and well-organized lobular architecture with clear visualization of cellular elements. The classical lobular structure was prominent, with centrally located central veins and radially oriented hepatocyte plates extending toward the portal tracts. Hepatocytes appeared uniform in size and shape, with moderately eosinophilic cytoplasm and centrally located round nuclei, often with distinctly visible nucleoli. Hepatocyte plates maintained the typical single- or double-row arrangement, and sinusoids were evenly distributed without signs of dilation, congestion, or collapse. Vascular elements, including the portal triads, were structurally intact and properly arranged, with no evidence of inflammatory infiltration, fibrosis, or parenchymal disruption. Along the sinusoids, occasional Kupffer cells were observed, reflecting normal phagocytic activity (Figure 3.2, panel A).

On the other hand, liver sections from the CCl_4-exposed untreated group displayed extensive parenchymal damage and near-complete loss of normal lobular organization. The typical radial arrangement of hepatic plates was largely absent, replaced by disorganized cellular clusters and collapsed sinusoidal spaces. Central veins were occasionally discernible but surrounded by distorted architecture and chaotic groups of hepatocytes. A hallmark feature was pronounced lipid degeneration affecting extensive areas of the parenchyma. Hepatocytes appeared enlarged and pale, often almost completely or fully replaced by large intracellular lipid vacuoles, frequently lacking visible nuclei. The widespread combination of macrovesicular and microvesicular steatosis imparted a monotonous and markedly degenerated appearance to the tissue. Many cells exhibited features of apoptosis or necrosis, including nuclear condensation, fragmentation, or complete loss; some vacuolated hepatocytes appeared as “ghost” remnants. Moderate mononuclear inflammatory infiltration was primarily localized to mid-zonal and centrolobular regions (Figure 3.2, panel B).

Liver sections from the Carsil-treated group showed restored lobular organization and a notable reduction in cytological damage compared to the untreated group, with only minimal residual alterations. Hepatic plates were more orderly arranged, with moderate uniformity in cell size and radial orientation from central to portal zones. Nevertheless, mild lipid degeneration was still present in individual hepatocytes or small clusters, characterized by small vacuolar changes that generally did not distort cellular morphology, though occasional more pronounced vacuolization was observed. Nuclei in affected or adjacent cells often displayed reactive changes, such as moderate enlargement, irregular contours, or prominent nucleoli, indicating persistent metabolic stress or regenerative activity.

AMERICAN JOURNAL OF APPLIED MEDICAL SCIENCE
ISSN: 2996-5101 (online) | ResearchBib (IF) = 10.81 IMPACT FACTOR
Volume-3| Issue-8| 2025 Published: |30-09-2025|

Most surrounding hepatocytes retained moderately eosinophilic cytoplasm and centrally located round nuclei without signs of irreversible damage. Sinusoids were evenly distributed, maintaining nearly normal lumen and spacing, without evidence of collapse or hemorrhagic alterations. Mononuclear infiltrates were sparse and diffusely distributed, lacking the dense clusters observed in the untreated group (Figure 3.2, panel C).

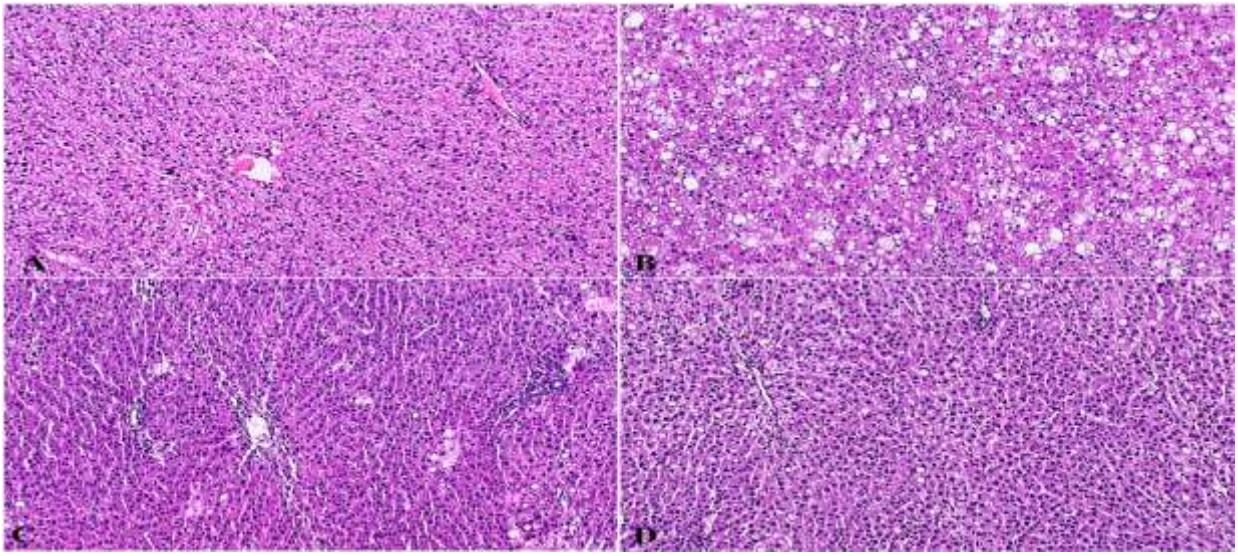

Figure 3.2. Representative liver histology at intermediate magnification across all experimental groups..

At intermediate magnification, liver sections from the Rutan-treated group exhibit largely restored hepatic architecture, with clearly defined lobular organization, distinctly visible central veins, and regularly arranged hepatocyte plates. This pattern is similar to that observed in the Carsil-treated group; however, the Rutan-treated sections show slightly more uniform organization in the midzonal region and orderly sinusoidal distribution. Mild steatotic changes persist in individual hepatocytes or small clusters, manifested as small or moderately sized vacuoles, which do not cause significant distortion of cellular structure. The degree of lipid accumulation is comparable to or slightly higher than in the Carsil group. Some hepatocytes display reactive nuclear changes, such as karyomegaly or prominent nucleoli, indicative of localized regeneration rather than ongoing damage. Inflammatory infiltrates are minimal and diffusely distributed, without dense foci or sinusoidal clustering, similar to the Carsil group. Sinusoids remain evenly spaced, without signs of collapse or congestion (Figure 3.2, panel D).

At high magnification (objective ×40), liver tissue from the intact control group displays uniform hepatocyte morphology: cells are polygonal, with moderately eosinophilic granular cytoplasm and centrally located round nuclei containing fine-grained chromatin and prominent nucleoli. Hepatocyte plates form one- to two-

cell-thick trabeculae, separated by regular sinusoidal capillaries lined with flattened endothelial cells and occasional Kupffer cells. Cell membranes remain intact, with no signs of cytoplasmic vacuolization, lipid accumulation, or necrosis. Sinusoids and vascular structures maintain normal lumen and orderly arrangement, with no evidence of inflammatory infiltration or congestion. Portal tracts are structurally preserved, containing clearly identifiable bile ducts, portal venules, and hepatic arterioles, surrounded by minimal connective tissue (Figure 3.3, panel A).

In contrast, liver parenchyma from the CCl_4-exposed untreated group exhibits pronounced cytological heterogeneity and clear signs of progressive hepatocyte degeneration. Cells contain numerous cytoplasmic vacuoles of varying sizes, indicative of both macro- and microvesicular steatosis. Lipid inclusions displace cytoplasmic contents and frequently push nuclei toward the periphery. Many hepatocytes are enlarged and pale, with clearly defined lipid droplets, while others retain eosinophilic granular cytoplasm, reflecting transitional stages between steatosis and injury. The presence of anucleated hepatocytes, often with large lipid vacuoles, indicates progression toward lipid-induced apoptosis or necrosis. These cells show cytoplasmic condensation or fragmentation, confirming irreversible damage. Nuclear changes include pyknosis, karyorrhexis, and complete loss of nuclei, while some hepatocytes retain intact nuclei with prominent nucleoli, producing a mosaic pattern of injury. Mononuclear inflammatory infiltrates, mainly lymphocytes and monocyte-like cells, are observed within sinusoids and surrounding degenerating hepatocytes, reflecting localized immune activation. In some areas, Kupffer cells appear enlarged, indicating increased phagocytic activity. In the most severely affected regions, disintegration of hepatocyte plates is accompanied by sinusoidal dilation and partial tissue collapse, resulting in disorganized cellular clusters replacing the normal radial architecture (Figure 3.3, panel B).

AMERICAN JOURNAL OF APPLIED MEDICAL SCIENCE
ISSN: 2996-5101 (online) | ResearchBib (IF) = 10.81 IMPACT FACTOR
Volume-3| Issue-8| 2025 Published: |30-09-2025|

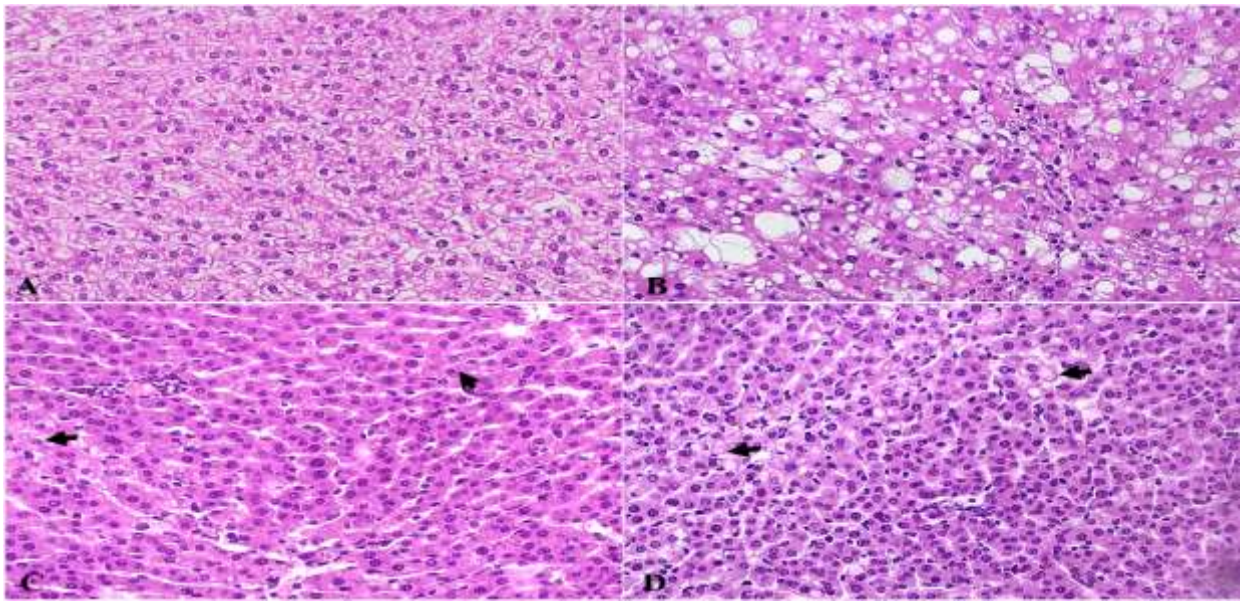

Figure 3.3. Representative liver histology at high magnification across all experimental groups.

At high magnification, liver sections from the Carsil-treated group exhibit relatively homogeneous hepatocyte morphology. Most cells display moderately eosinophilic cytoplasm with well-defined, centrally located nuclei. Widespread cytoplasmic vacuolization, prominent in the untreated group, is markedly reduced, and macrovacuolar steatosis is absent. Only occasional hepatocytes contain small, pale cytoplasmic vacuoles indicative of limited microvesicular changes, without significant nuclear displacement or cytoplasmic swelling. Signs of irreversible damage—such as anucleated cells, pyknotic nuclei, karyorrhexis, or karyolysis—are minimal and occur far less frequently than in the untreated group. Most hepatocyte nuclei appear intact, round, uniformly stained, and with clearly visible nucleoli, reflecting preserved nuclear architecture. Nuclear morphology remains relatively uniform, without the cytological heterogeneity observed in CCl_4-exposed untreated livers. Mononuclear inflammatory cells, abundant in the untreated group, are observed only sporadically or in small aggregates within the sinusoids, without forming dense perisinusoidal or lobular foci characteristic of active infiltration. Furthermore, no hypertrophy or clustering of Kupffer cells is detected, indicating minimal or resolved macrophage activation. The organization of hepatocyte plates and interplate sinusoids is generally preserved: sinusoids maintain a uniform lumen, hepatocytes are radially arranged, and there are no signs of collapse or architectural disarray typical of severely damaged regions in the untreated group (Figure 3.3, panel C).

In liver sections from rats treated with Rutan (the experimental compound), stained with hematoxylin and eosin and examined at high magnification cellular features are generally comparable to those observed in the Carsil-treated group,

AMERICAN JOURNAL OF APPLIED MEDICAL SCIENCE
ISSN: 2996-5101 (online) | ResearchBib (IF) = 10.81 IMPACT FACTOR
Volume-3| Issue-8| 2025 Published: |30-09-2025|

although localized variability in the extent of residual liver damage is noted. Lobular architecture is largely preserved, hepatocytes are polygonal with distinct cell borders, and nuclei are centrally located. In most areas, hepatocyte morphology, nuclear structure, and sinusoidal organization are similar to the Carsil group, indicating a comparable effect of Rutan on the progression of toxic liver injury. However, in some focal areas, large cytoplasmic vacuoles are observed in hepatocytes, indicating the persistence of lipid degeneration (macrovacuolar steatosis). These changes are limited in scope and occur in localized foci (Figure 3.3, black arrows in panel D), likely reflecting the consequences of prior toxic exposure. Certain regions exhibit more pronounced vacuolization compared to neighboring areas. At the nuclear level, most hepatocytes retain normal morphology; however, some cells display reactive changes, including prominent nucleoli and irregular nuclear contours. These alterations are focal and may represent residual cellular stress or early regenerative responses. Compared with the Carsil group, these nuclear changes are slightly more noticeable in some areas, though in other regions no differences are observed. Sinusoidal dilation and inflammatory infiltration are minimal and comparable in intensity to the Carsil group, indicating no substantial differences in vascular or immune responses (Figure 3.3, panel D).

Morphometric quantitative analysis was performed to objectively assess the severity of liver injury and the efficacy of therapeutic interventions across the different experimental groups. Key histological parameters—including mononuclear cell infiltration (Figure 3.4, panel A), steatotic area (Figure 3.4, panel C), and the number of hepatocytes containing lipid inclusions or exhibiting nuclear damage (Figure 3.4, panel D)—were systematically measured at standardized magnification in randomly selected fields.

AMERICAN JOURNAL OF APPLIED MEDICAL SCIENCE
ISSN: 2996-5101 (online) | ResearchBib (IF) = 10.81 IMPACT FACTOR
Volume-3| Issue-8| 2025 Published: |30-09-2025|

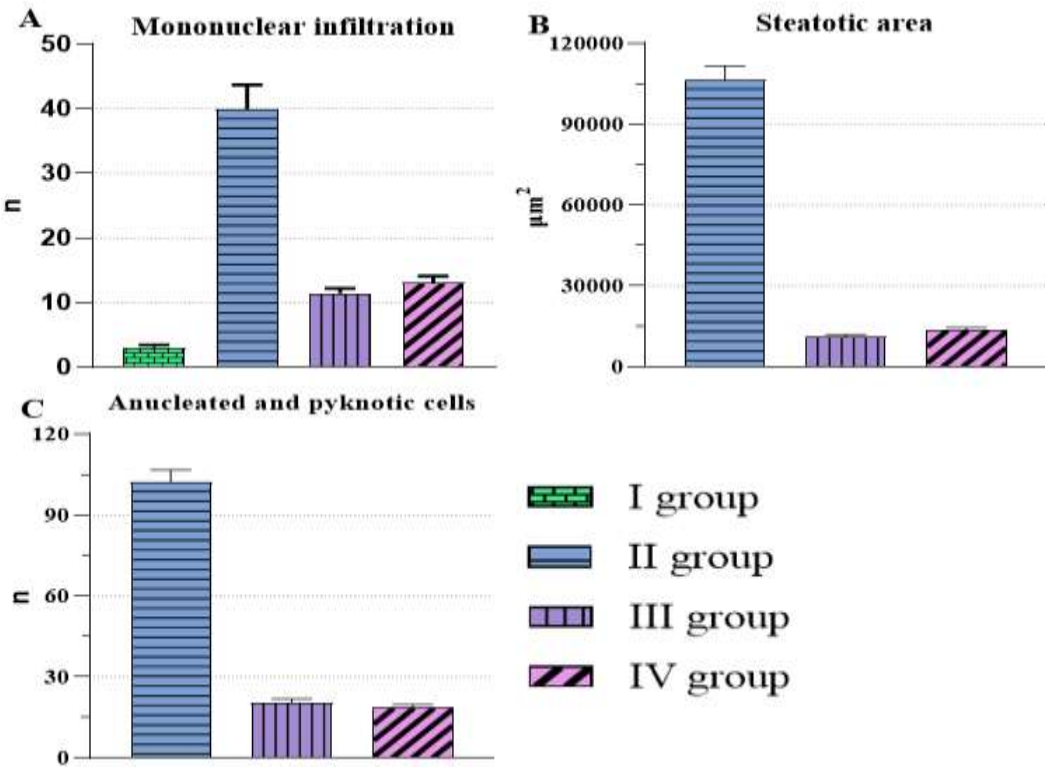

Figure 3.4. Morphometric assessment of liver tissue damage and treatment effects: (A) Quantitative evaluation of mononuclear cell infiltration in liver tissue; (B) Quantitative analysis of steatotic (lipid) areas in the liver parenchyma following CCl_4-induced injury; and (C) Quantitative assessment of hepatocytes containing lipid inclusions with anuclear or pyknotic nuclei across the experimental groups.

Quantitative assessment of mononuclear cell infiltration at intermediate magnification revealed pronounced intergroup differences. In the intact control group (Group I), the mean number of mononuclear cells was low (3.08 ± 0.34 cells, n), consistent with normal liver histology and the absence of an inflammatory response (Figure 3.4, panel A). In contrast, the CCl_4-exposed untreated group (Group II) exhibited a marked increase in mononuclear cell numbers (39.92 ± 3.76 cells, n; $p < 0.0001$ versus Group I), reflecting a pronounced inflammatory reaction following acute toxic liver injury. Both treatment groups—Carsil (Group III: 11.42 ± 0.76 cells, n) and Rutan (Group IV: 13.08 ± 1.02 cells, n)—showed a significant reduction in mononuclear cell infiltration compared to Group II ($p < 0.0001$), indicating a substantial anti-inflammatory effect in response to therapy. However, mononuclear cell counts in Groups III and IV remained significantly higher than in the intact control group ($p < 0.0001$), suggesting incomplete regression of the inflammatory process. Notably, no statistically significant differences were observed between the Carsil and Rutan groups ($p > 0.05$), indicating comparable anti-inflammatory efficacy of both agents in this experimental model.

Morphometric assessment of hepatic steatosis was performed by measuring the area of parenchyma affected by lipid accumulation at low magnification (Figure

3.4, panel B). Various regions of the hepatic lobule were considered, with particular attention to the midzonal areas, which are known to be most susceptible to toxic injury. Only zones with clearly defined steatotic changes—predominantly macrovesicular or conglomerated microvesicular lipid accumulation—were included in the analysis. In the untreated CCl_4-exposed group (Group II), the mean area affected by lipid inclusions reached 106,686.25 ± 4,948.25 μm², reflecting pronounced hepatocellular lipid dystrophy and confirming the severity of steatotic damage induced by the toxin. In contrast, treatment with both Carsil (Group III) and Rutan (Group IV) substantially reduced the extent of lipid accumulation. In the Carsil-treated group, the mean affected area was only 11,016 ± 943.22 μm², whereas in the Rutan-treated group it was 13,796 ± 721.18 μm². Statistical analysis demonstrated that both treatments significantly decreased steatosis compared to the untreated group ($p < 0.0001$), confirming the lipid-modulating effect of these therapeutic agents. Moreover, a statistically significant difference was observed between the two treatment groups: the Carsil group (Group III) exhibited a smaller steatotic area than the Rutan group (Group IV) ($p < 0.0001$), indicating a relatively higher efficacy of Carsil in reducing hepatocellular lipid accumulation.

Quantitative assessment of hepatocytes exhibiting pronounced lipid accumulation and nuclear abnormalities—such as pyknosis or complete nuclear loss—revealed significant intergroup differences (Figure 3.4, panel C). In the untreated CCl_4-exposed group (Group II), the number of severely damaged hepatocytes was markedly elevated (102.25 ± 4.53 cells), reflecting extensive hepatocellular degeneration due to toxic injury. Experimental therapy with Carsil (Group III) led to a statistically significant reduction in the number of damaged hepatocytes (17.67 ± 1.08 cells; $p < 0.0001$ vs. Group II), indicating a pronounced protective effect. An even greater reduction was observed in the Rutan-treated group (Group IV: 14.25 ± 1.05 cells; $p < 0.0001$ vs. Group II), demonstrating more effective preservation of hepatocytes. Furthermore, the difference between Groups III and IV was statistically significant ($p < 0.05$): the Rutan group exhibited fewer lipid-laden hepatocytes with anuclear or pyknotic nuclei. This suggests that Rutan may exert a more pronounced hepatoprotective effect than Carsil at the cellular level in the context of CCl_4-induced liver injury.

Conclusion. Morphological analysis demonstrated that both Carsil and Rutan treatment resulted in pronounced structural improvement of the liver following CCl_4-induced injury, including reductions in hepatocellular lipid accumulation, inflammatory infiltration, and overall architectural disorganization. Vascular structures in both groups remained intact, with relatively normalized sinusoidal architecture and preserved lobular organization. While certain histological

features—such as hepatocyte alignment and microcirculatory spacing—appeared slightly more regular in Rutan-treated samples, livers from Carsil-treated animals exhibited fewer areas with lipid inclusions and localized dystrophy. Nevertheless, no clear or consistent morphological superiority of one compound over the other was observed. These findings indicate that both agents exert a comparable hepatoprotective effect at the structural level.

Morphometric assessment revealed that both Carsil and Rutan significantly reduced the severity of CCl_4-induced steatosis, cellular degeneration, and inflammation. In Carsil-treated animals, the area of parenchyma affected by lipid accumulation was smaller compared to the Rutan group, indicating a higher efficacy of Carsil in limiting the tissue-level spread of steatosis. However, in Rutan-treated rats, the number of severely damaged hepatocytes—specifically lipid-laden cells with anuclear or pyknotic nuclei—was lower, reflecting more effective protection against lipid-induced cellular injury. These results suggest that, while Carsil more effectively restricts the extent of tissue-level steatosis, Rutan better preserves hepatocyte integrity at the single-cell level. Collectively, both compounds confer beneficial effects, though their hepatoprotective profiles may differ in focus: tissue-level limitation of steatosis in the case of Carsil versus cellular resilience to lipid-associated damage in the case of Rutan.

REFERENCES:

1. https://www.who.int/news/item/09-04-2024.
2. Determination of anti-influenza activity of polyphenol-based plant-derived preparations. Medical Journal of Uzbekistan. 2007; (5): 64–67.
3. Aripov T.F., Ghaibov U.G., Ghaibova S.N., Ugli Abdullaev A.A., Kizi Abduazimova D.Sh., Oshchepkova Yu.I., Salikhov Sh.I. Antioxidant and antiradical activity in vitro of the sum of polyphenols (substance of the antiviral drug Rutan) from the leaves of the tannin sumac
4. Rhus coriaria L. Chemistry of Plant Raw Materials. 2024; (4): 138–147. Abzalov Sh.R., Khakimov Z.Z., Rakhmanov A.Kh. The effect of dry extract obtained from Rhus coriaria in experimental models of edema and inflammation. American Journal of Medicine and Medical Sciences. 2020; 10(7): 503–508.
5. Khakimov Z.Z., Rakhmanov A.Kh., Abzalov Sh.R. The effect of leaf extract from Rhus coriaria L. on the course of chronic arthritis. Medical Journal of Uzbekistan. 2024; (2): 182–188.

6. Boboeva R.R., Mavlonov A.A., Jurayeva G.B. Choleretic activity of Rutana at therapeutic application in rats with heliotrin hepatitis. European journal of molecular & clinical medicine, 2020. – volume 7. – P. 5188-5193.

7. Mavlonov A.A., Boboeva R.R. Study of the hepatoprotective action of Rutan. Academicia: an international multidisciplinary research journal. 2020; 10(5):117-120.

8. Matveev A.V. Hepatoprotectors: Analysis of International Studies on Liver Drug Preparations. Simferopol: IT "ARIAL," 2013. 384 p.

9. Khakimov Z.Z., Khalmuratova F.A., Rakhmanov A.Kh. Experimental Assessment of the effect of Rutan on the level of endogenous intoxication syndrome in prepubertal an. Texas Journal of Medical Science. https://zienjournals.com August 2025; Vol. 47:1-6.

10. Khakimov Z.Z., Rakhmanov A.Kh., Khalmuratova F.A. Evaluation of the effectiveness of Rutan and Karsil in correcting antipyrine pharmacokinetics disorders in rabbits with acute toxic hepatitis during the growth period. American Journal of Pediatric Medicine and Health Sciences.2025; 3(7):108-112. https://grnjournal.us/index.php/AJPMHS/article/view/8164.

11. KhakimovZ.Z., Rakhmanov A.Kh., Khalmuratova F.A. Study of the effect of Rutan and Karsil on the absorptive-excretory function of the liver in acute toxic hepatitis during the prepubertal period. Web of Medicine: Journal of Medicine, Practice and Nursing. ISSN (E): 2938-3765. webofjournals.com/index.php/5.2025; 3(7):70-76.

12. KhakimovZ.Z., Rakhmanov A.Kh., Khalmuratova F.A. The effect of Rutan on the biochemical blood parameters of prepubertal rabbits with acute toxic hepatitis. Journal of medicine and pharmacy. |20-05-2025|. Volume-8, Issue-5, P.12-19. Published https://doi.org/10.5281/zenodo.16904112.

13. Mironov A.N. Guidelines for Conducting Preclinical Studies of Medicinal Products. Part One. Moscow: Grif i K, 2012. 944 p.